Electronic structure of $Bi_2CaSr_2Cu_2O_8$ determined by a combined analysis of various polarized x-ray-absorption spectra

Antonio Bianconi, Chenxi Li,* and Stefano Della Longa
University of L'Aquila, via San Sisto 20, 67100 L'Aquila, Italy
and Dipartimento di Fisica, Università degli Studi di Roma "La Sapienza," I-00185 Roma, Italy

Margherita Pompa
Dipartimento di Fisica, Università degli Studi di Roma "La Sapienza," I-00185 Roma, Italy
and Laboratoire pour l'Utilisation du Rayonnement Electromagnétique (LURE), Université de Paris—Sud, Bâtiment No. 209D, 91405 Orsay CEDEX, France
(Received 22 March 1991)

The polarized E⊥c oxygen K-edge x-ray-absorption near-edge structure (XANES) spectrum of $Bi_2Sr_2CaCu_2O_{8+\delta}$ (Bi 2:2:1:2) has been calculated by a multiple-scattering approach and compared with experimental data. The symmetry of the conduction bands over a range of 15 eV above the Fermi level has been studied by a combined analysis of five different polarized x-ray-absorption spectra at the following edges: O K edge, Cu K edge, and Cu L_3 edge. Information on the partial density of states of the conduction bands, $\mathcal{D}_{X(l,m_l)}$, projected on the atomic site X (Cu and O) with selected orbital angular momentum l, and its projection m_l along the c axis ($\mathcal{D}_{\mathrm{Cu}(2,0)}$, $\mathcal{D}_{\mathrm{Cu}(2,\pm1)}$, and $\mathcal{D}_{\mathrm{Cu}(2,\pm2)}$ for the Cu site; $\mathcal{D}_{\mathrm{O}(1,0)}$ and $\mathcal{D}_{\mathrm{O}(1,\pm1)}$ for the oxygen site) have been obtained. The symmetry of the itinerant states induced by doping at the Fermi level is deduced to be a mixture of $3d$ holes with $m_l=\pm2$ and $m_l=0$ orbital angular momenta and holes on planar oxygen in the molecular-orbital combination of local b_1 and a_1 symmetry [the ligand holes $\underline{L}(b_1)$ and $\underline{L}(a_1)$].

I. INTRODUCTION

The anomalous electronic structure of superconducting cuprate perovskites has been a subject of substantial interest in attempts to understand the pairing mechanism leading to high-T_c superconductivity. The presence of a large hole-hole Coulomb repulsion $U_{dd}\sim6$ eV has been found by x-ray photoelectron spectroscopy,[1-3] resulting in an inadequacy of the standard description of the states at the Fermi level in terms of the one-electron approximation.[4-6] The quantitative picture of the electronic states remains an open problem because of the lack of a microscopic theoretical description of the electronic states at the Fermi level (including the electron-phonon interaction) which is able to predict all anomalous properties of these metals detected by different experimental methods. The absence of the itinerant Cu $3d^8$ states and the formation of $3d^9\underline{L}^*$ states by doping have been found experimentally by Cu L_3 x-ray-absorption spectroscopy in $YBa_2Cu_3O_{\sim7}$ (Ref. 7) and in $La_{1.85}Sr_{0.15}CuO_4$ (Ref. 8) and confirmed by many experiments. The controversy remains on the nature of the $3d^9\underline{L}$ at the Fermi level induced by doping.

Some authors have focused only on the Cu $3d_{x^2-y^2}$ and the O $2p_{x,y}$ orbitals as describing the local spins responsible for antiferromagnetism as well as the carriers. This point of view is the basis of the three-band extended Hubbard model that has been extensively studied including electronic correlations.[9-11] This model describes the itinerant states at the Fermi level as the first ionization states in a CuO_2 layer of the insulating parent compound that mainly consist of one hole in the Cu $3d_{x^2-y^2}$ orbital (b_1 symmetry) and of another one in a linear combination of four oxygen σ bonding orbitals also with b_1 symmetry, the so-called Zhang-Rice $3d^9_{x^2-y^2}\underline{L}(b_1)$ singlet states.[11] The nearly pure x,y polarization of the O $1s\rightarrow2p$ transitions to the states at the Fermi level at the O K-edge absorption threshold of Bi cuprates[12-14] has been assumed as giving experimental support to the three-band model.

Other authors have proposed different models where the $3d^9\underline{L}^*$ states induced by doping are different from the first ionization states $3d^9_{x^2-y^2}\underline{L}(b_1)$ of the insulating parent compound. These models assume a nonrigid electronic structure of the states at the Fermi level with doping. Experimental evidence for this model was given in the early times of the research on cuprate superconductors by the Cu L_3 x-ray-absorption spectroscopy[8] where the polarization dependence shows (i) the presence of a $3d_{3z^2-r^2}$ component of the Cu $3d$ holes modulated by the doping level in all cuprate superconductors,[15,16] and (ii) the presence of oxygen holes on the O $2p_z$ orbitals of the apical oxygen O(apical) in $YBa_2Cu_3O_{\sim7}$,[15] also if this last system seems to be unique among the families of high-T_c superconductors. In agreement with this model, the states induced by doping have been described as a sort of impurity band growing in the correlation gap.[17]

Several theories for the pairing mechanism based on this model,[18-23] which consider the presence of two bands with different symmetry around the Fermi level and electron-phonon coupling via the pseudo-Jahn-Teller effect,[16] have been proposed. The modulation of the orbital angular momentum m_l (or simply, m) of the Cu $3d$ holes by charge carriers can drive a large electron-phonon coupling which motivated Bednorz and Müller[24]

 ©1992 The American Physical Society

in their work that led to the discovery of high-T_c superconductivity.

In order to resolve the present controversy it is necessary to develop some quantitative data analysis of the experiments probing the orbital angular momentum of the holes in high-T_c superconductors. X-ray-absorption spectroscopy provides a direct probe of the orbital angular momentum via the dipole selection rules of the electronic transitions from deep core levels of well-defined atomic symmetry. In the case of metallic cuprate perovskites, this is a unique direct experimental method providing this key information: ESR (electron-spin-resonance) spectroscopy is inapplicable in this case; because the absolute value of the magnetic hyperfine shift in NMR (nuclear-magnetic-resonance) spectroscopy depends both on the atomic Cu $3d$ orbital angular momentum and on crystalline effects, it cannot be used to measure the change of the $3d$ orbital angular momentum from the insulating to the metallic phase.

The use of the x-ray-absorption spectroscopy to determine the unoccupied-electronic-state band structure is limited by final-state effects. In fact, the core hole induces an excitonic shift on the valence-band states, which is different for different final valence-band states and/or initial core states. In this work we propose a method to determine the structure of the unoccupied electronic states from a combined analysis of several x-ray-absorption spectra.

First, the polarized absorption cross sections of the atomic species of the crystal and of different core levels of each atom are calculated by the multiple-scattering approach. The calculation is carried out in an unperturbed potential describing the ground-state properties. Each conduction band will give peaks in the theoretical absorption spectra at slightly different energies because the peaks in each partial and local density of states occur at different energies. Therefore, the different calculated final states reached in each spectrum can be aligned on the same energy scale.

Second, the absorption cross sections are calculated including the effect of the core hole in the final state. This allows one to estimate the excitonic shift for each electron-hole final state relative to the energy position calculated in the first step.

Third, the experimental spectra are compared with the calculated spectra, including the core hole and the photoelectron lifetime. The experimental and the theoretical spectra are aligned on the same energy scale by looking for the best agreement among several features of the x-ray-absorption near-edge structure (XANES) over a large energy range above the Fermi level where the core hole effect induces only a nearly rigid shift of the spectrum.

This procedure allows the alignment of the different experimental absorption spectra on the same energy scale and the assignment of the final states in each spectrum to the unoccupied bands in the ground state.

We have applied this method to investigate the unoccupied states above the Fermi level in $Bi_2Sr_2CaCu_2O_{8+\delta}$ (Bi 2:2:1:2) which exhibits superconductivity with a critical temperature in the range 70–90 K. This material has been the subject of extensive experimental investigations. The dispersion of the bands near the Fermi level has been measured by angle-resolved photoemission.[25–28] The angle-resolved photoemission data show a band crossing the Fermi level in the Γ-X direction and at the saddle point in the Γ-M direction where mixing with the BiO bands is expected to be large on the basis of the one-electron band calculations.[29–33] The presence of two different bands crossing the Fermi level[25] in the photoemission spectra is controversial. The unoccupied electronic states have been investigated by infrared,[34,35] vacuum ultraviolet reflectivity,[35] electron-energy-loss,[36] and inverse photoemission[37] spectroscopies.

Here we have focused our attention on both the Cu and O x-ray-absorption spectra of the Bi 2:2:1:2 crystal in order to extract the electronic structure of the CuO_2 planes relevant to superconductivity. The x-ray-absorption spectra are determined by electronic transitions from a selected atomic core level to the unoccupied valence-band states above the Fermi level that is given, according to the Fermi Golden Rule, by the product of the matrix element $\mathcal{M}(\omega)$ and the selected partial density of valence-band states $\mathcal{D}_{l,m}$ with the orbital angular momentum quantum numbers l and m (or m_l) projected on the atomic site of the absorbing atom: $\alpha(\omega) \propto \mathcal{M}_{L_i,L_f}(\omega)\mathcal{D}_{l,m}(\omega)$, where $L_i \equiv (l_i, m_i)$ and $L_f \equiv (l_f, m_f)$ indicate the orbital angular momentum quantum numbers (l,m) of the initial (i) and final (f) states. Therefore, the absorption spectrum of a single level in a single atom X gives only partial information on the unoccupied density of states $\mathcal{D}_{X(l,m)}$. In order to have a complete picture of the symmetry of the unoccupied states in a system formed by several atomic species, it is necessary to perform a combined analysis of the absorption spectra of the different atoms and different core levels.

The dipole selection rule $\Delta l = l_f - l_i = \pm 1$ for the core transitions from the atomic levels Cu $1s$ or O $1s$ with angular momentum $l_i = 0$ selects the partial density of states with angular momentum $l_f = 1$ (p-like density of states) in both Cu and O K-edge spectra. In the Cu L_3-edge spectrum, the dipole selection rule $\Delta l = +1$ from the Cu $2p$ ($l_i = 1$) initial state selects the $l_f = 2$ final states (the d-like density of states). Because the cross section for the Cu $2p \rightarrow s$ channel allowed by the $\Delta l = -1$ selection rule has an oscillator strength a factor 100 smaller than the Cu $2p \rightarrow 3d$ transition, it can be neglected.[38]

The polarized absorption spectra provide additional information on the z components (the z axis is chosen parallel to the c axis of the Bi 2:2:1:2 crystal) of the orbital angular momentum m_l of the unoccupied conduction states.

The dipole selection rules for the polarized x-ray-absorption spectra are determined by the integral over three spherical harmonics

$$\sum_{m_i} |\langle Y_{l_i,m_i}(\hat{\mathbf{r}}) | Y_{l_\gamma,m_\gamma}(\hat{\mathbf{r}}) | Y_{l_f,m_f}(\hat{\mathbf{r}}) \rangle|^2 ,$$

where $Y_{l_i,m_i}(\hat{\mathbf{r}})$ describes the core initial state, $Y_{l_f,m_f}(\hat{\mathbf{r}})$ the electron final state, and $Y_{l_\gamma,m_\gamma}(\hat{\mathbf{r}})$ the polarized pho-

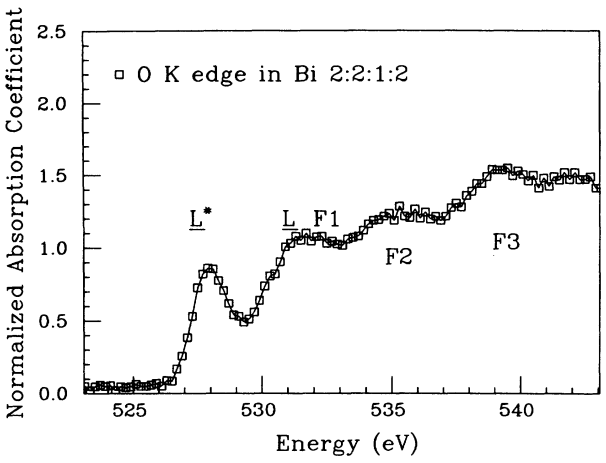

FIG. 1. Polarized E⊥c O K-edge XANES spectra of $Bi_2Sr_2CaCu_2O_{8+\delta}$ from Ref. 39.

ton field. This integral is proportional to the 3-j Wigner symbols

$$\begin{pmatrix} l_i & l_\gamma & l_f \\ m_i & m_\gamma & m_f \end{pmatrix}^2 ,$$

which are different from zero under the condition that $m_i+m_\gamma+m_f=0$.

This additional dipole selection rule in the E||z polarized K-edge absorption spectra selects only the p-like ($l=1$) states with orbital angular momentum $m_l=0$ ($2p_z$), while in the E⊥z polarization only the p-like ($l=1$) final states with orbital angular momentum $m_l=\pm1$ ($2p_{x,y}$) are reached.

Unique information on the orbital angular momentum $m_l=0,\pm1,\pm2$ of the $l=2$ (Cu d-like) unoccupied partial density of states can be extracted by polarized L_3-edge XANES spectroscopy.[38] In fact, the dipole selection rules select the unoccupied d-like ($l=2$) density of valence-band states projected on Cu site with orbital angular momentum $m_l=0,\pm1$ in the E||z spectra, and with $m_l=0,\pm1,\pm2$ in the E⊥z spectra.

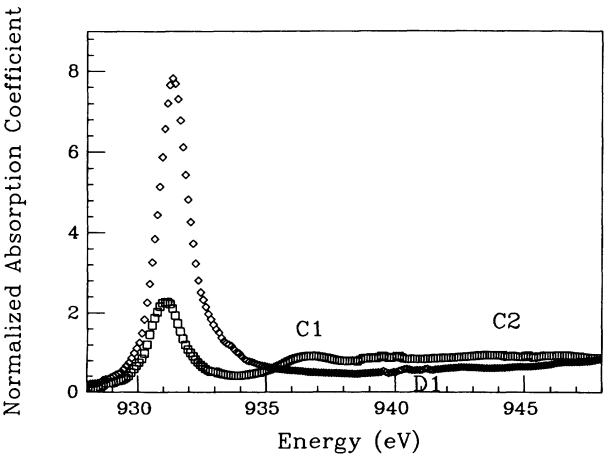

FIG. 2. Polarized E⊥c (diamonds) and E||c (squares) Cu L_3-edge XANES spectra of $Bi_2Sr_2CaCu_2O_{8+\delta}$ measured in the total electron yield mode (from Ref. 38).

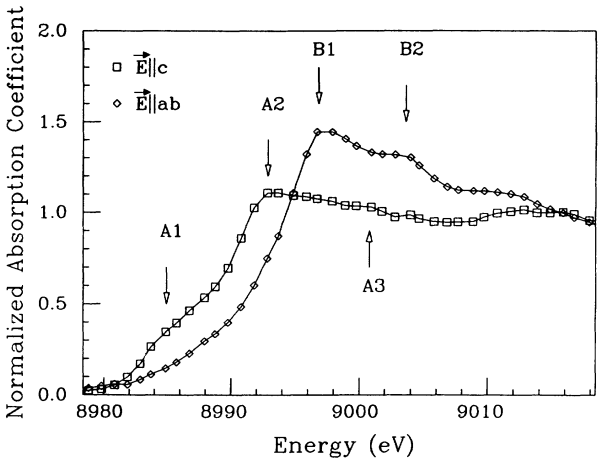

FIG. 3. Polarized E⊥c (or E||ab plane) (diamonds) and E||c (squares) Cu K-edge XANES spectra of $Bi_2Sr_2CaCu_2O_{8+\delta}$ from Ref. 40.

We have analyzed here the polarized x-ray-absorption spectra at the oxygen K edge (~528 eV), Cu L_3 edge (~931 eV), and Cu K edge (~8980 eV) of Bi 2:2:1:2 crystals. Because of the large difference in each core-level binding energy, the absorption spectra occur in a different photon spectral range requiring different monochromators and synchrotron radiation beam lines.

The E⊥c polarized oxygen K-edge absorption spectrum of Bi 2:2:1:2 has been measured by Krol *et al.*[39] (see Fig. 1) by means of a bulk-sensitive detection method, the $K\alpha$ soft x-ray fluorescence yield, at the National Synchrotron Light Source, Brookhaven National Laboratory.

The polarized Cu L_3 x-ray-absorption spectra (see Fig. 2) have been measured by using a double-crystal $10\bar{1}0$ beryl monochromator by using the super ACO synchrotron radiation source at the Laboratoire pour l'Utilisation du Rayonnement Electromagnétique (LURE), Orsay, France.[38] The absorption coefficient has been measured by total electron yield method.

The polarized Cu K-edge absorption spectra of Bi 2:2:1:2 crystals (see Fig. 3) (Ref. 40) have been measured by using the DCI storage ring at the Laboratoire pour l'Utilisation du Rayonnement Electromagnétique, Orsay, a double-crystal Si(331) monochromator and by recording the total electron yield.

II. JOINT ANALYSIS OF POLARIZED ABSORPTION SPECTRA

A. The oxygen K-edge absorption spectrum

The E⊥c oxygen K-edge absorption spectrum has been calculated in the real space by using the multiple-scattering formalism.[41–46] In this approach the transition rate from the atomic O 1s core level to the final states in the conduction bands with p-like character ($m_l=\pm1$) is calculated. The wave function of the excited electron is constructed in a potential having the form of nonoverlapping muffin tins with the absorbing O ion at its center. A cluster of 40 atoms with the planar oxygen O(planar) at its center has been created by using the atomic coordi-

nates given by Bordet *et al.*[47]

The calculation of the potential starts from the charge densities for neutral atoms on each site which were obtained by self-consistent-field atomic calculations of the relativistic Hartree-Fock-Slater kind. The charge densities about each atom were superimposed and spherically averaged. By solving Poisson's equation for the Coulomb part of the potential and adding a local exchange-correlation contribution of the $X\alpha$ type with $\alpha=1$, the spherically symmetric potentials in muffin-tin form were obtained. The intersphere energies near each atomic site i (the muffin-tin constants $\overline{V}_{0i}$) of the constructed muffin-tin potentials were initially determined by taking the average values of the potential in the space between the muffin-tin radius $R_{\mathrm{MT}i}$ and the radius of the Wigner-Seitz spheres. The muffin-tin radius of each atomic species has been chosen looking for a solution giving similar $\overline{V}_{0i}$ in order to minimize the variations of the interstitial potential about its mean value. The zero of the energy scale has been fixed at the Fermi level.

The calculated spectra are determined by the product of an atomiclike factor determined by the dipole-matrix element for the electronic transition from the oxygen $1s$ level to the continuum states in the muffin-tin potential of the isolated central Cu atom, $\alpha_0(\omega)$, and a factor determined by the partial density of states of the conduction bands projected on the absorbing atom X, $\mathcal{D}_{X(l,m)}$ that determines the modulation of the atomic absorption coefficient and it gives the interesting spectral features. The calculation of $\alpha_0(\omega)$ allows the normalization of the absorption coefficient to the high-energy value α_0 of the atomic absorption, i.e., $\alpha(\omega)/\alpha_0$. In this way the value of the calculated normalized absorption coefficient $\alpha(\omega)/\alpha_0$ is one for the atomic absorption jump of the absorption edge under study.

The calculated normalized absorption coefficient of the $\mathbf{E}\perp c$ oxygen K-edge spectrum is reported in Fig. 4(a). The zero of the energy scale is fixed at the calculated Fermi level E_0 indicated by an arrow. The transition rate to both occupied valence-band states and unoccupied conduction band is given. In the actual spectra only transitions to unoccupied states are allowed, but we have also reported in Fig. 4(b) the calculations for occupied states below the calculated Fermi level E_0 in order to show the full spectrum of the O $2p_{x,y}$ partial density of states contributing to the Cu derived valence band around the Fermi level as it comes out from the present one-electron calculation.

The main reason for this uncommon way to present the calculated XANES spectrum is that the present calculation is expected to be wrong near the Fermi level because of the electronic correlations within the Cu $3d$ derived states. Moreover, the range of energies where the electronic renormalization takes place is not well defined. Therefore, the position of the Fermi level E_0 is not expected to be correctly estimated by one-electron calculations and in the following part we will denote the calculated absorption threshold as the continuum threshold E_0 to distinguish it from the actual Fermi level in the real crystal, E_F. The calculated continuum threshold E_0 crosses a continuum flat spectrum of O $2p_{x,y}$ density of states extending from -4 below to $+4$ eV above the Fermi level.

The final states O $2p_{x,y}$ of the planar oxygen atoms O(planar) that contribute to the calculated cross section

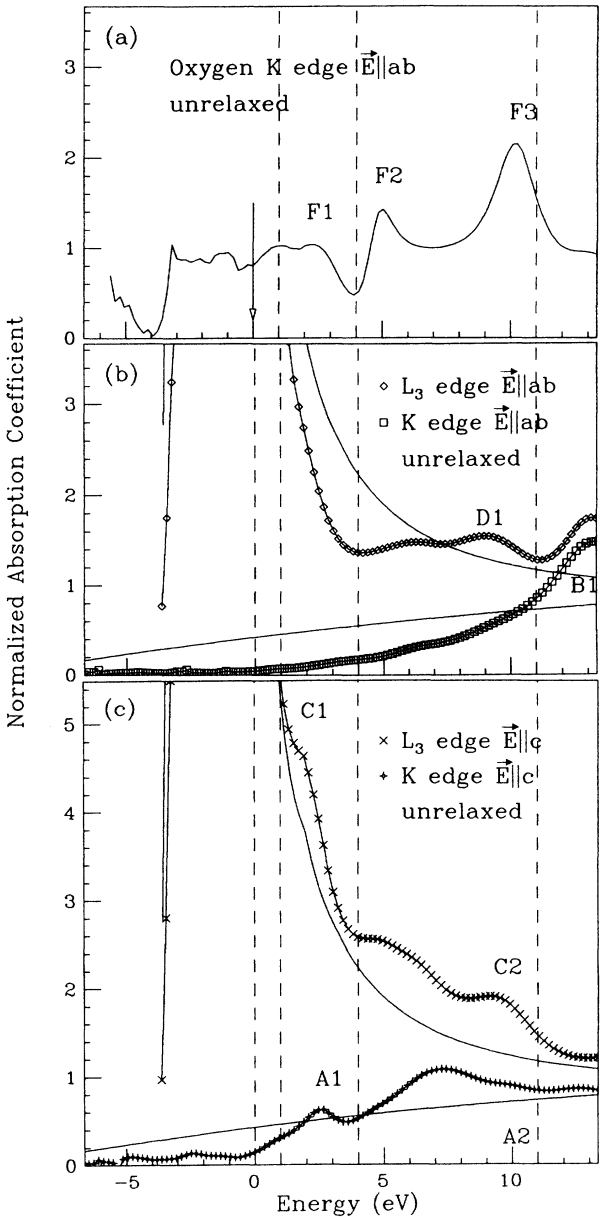

FIG. 4. (a) Calculated polarized $\mathbf{E}\perp c$ ($\mathbf{E}\|ab$ plane) O K-edge XANES spectra of the planar oxygen O(planar) in the CuO_2 plane in the unrelaxed potential of $Bi_2Sr_2CaCu_2O_8$. (b) Calculated polarized $\mathbf{E}\perp c$ ($\mathbf{E}\|ab$ plane) Cu K-edge and Cu L_3-edge XANES spectra in the unrelaxed potential. The atomic absorption spectra $\alpha_0(\omega)$ for the Cu $1s\rightarrow\varepsilon p$ and for the Cu $2p\rightarrow\varepsilon d$ transitions are plotted (solid lines). (c) Calculated polarized $\mathbf{E}\|c$ Cu K-edge and Cu L_3-edge XANES spectra in the unrelaxed potential. The atomic absorption spectra $\alpha_0(\omega)$ for the Cu $1s\rightarrow\varepsilon p$ and for the Cu $2p\rightarrow\varepsilon d$ transitions are plotted (solid lines). The zero of the energy scale is fixed at the calculated Fermi energy level E_0 in the present one-electron calculations. Both transitions to occupied (below the Fermi level E_0) and unoccupied valence-band states (above the Fermi level E_0) have been calculated.

from the O 1s level in the calculated E⊥c oxygen K edge are derived by three sets of molecular orbitals: (i) The b_1 molecular orbitals $\underline{L}(b_1)$ formed by the molecular orbital combination of the O $2p_{x,y}$ orbitals of the four planar oxygens coordinated by Cu in the CuO_2 layer with the molecular orbital combination of local b_1 symmetry $(1/\sqrt{4})(+p_{x1}-p_{y2}-p_{x3}+p_{y4})$ that are mixed with the Cu $3d_{x^2-y^2}$ orbitals, where the phases of the orbitals have been chosen with the same standard convention used in Ref. 48; (ii) the a_1 molecular orbitals $\underline{L}(a_1)$ formed by the molecular orbital combination of the O $2p_{x,y}$ orbitals of the four planar oxygen atoms coordinated by Cu in the CuO_2 layer with the molecular orbital combination of local a_1 symmetry $(1/\sqrt{4})(+p_{x1}+p_{y2}-p_{x3}-p_{y4})$ that are mixed with the Cu $3d_{3z^2-r^2}$ orbital; (iii) the b_2 molecular orbitals $\underline{L}(b_2)$ formed by the molecular orbital combination of the O $2p_{x,y}$ orbitals of the four planar oxygens coordinated by Cu in the CuO_2 layer with the molecular orbital combination of local b_2 symmetry $(1/\sqrt{4})(+p_{y1}+p_{x2}-p_{y3}-p_{x4})$ that are mixed with Cu $3d_{xy}$ orbitals.

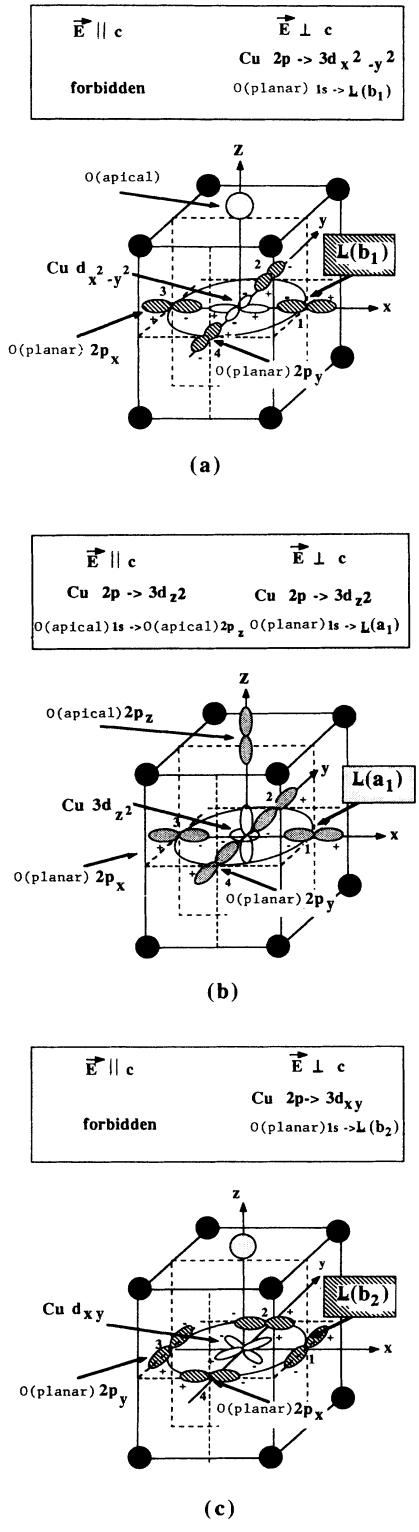

FIG. 5. Schematic picture of the final valence-band states of symmetry (a) b_1, (b) a_1, and (c) b_2 that can be reached with polarized Cu L_3-edge and O K-edge absorption.

The E∥c oxygen K-edge spectrum is not discussed here, it will probe the electronic transitions (1) to the final states $\underline{L}(e)$ formed by the O $2p_z$ components of the planar oxygen atoms O(planar) mixing with the Cu $3d_{xz}$ and Cu $3d_{yz}$ orbitals with the e symmetry $(1/\sqrt{2})(+p_{z1}-p_{z3})$, $(1/\sqrt{2})(p_{z2}-p_{z4})$, and (2) to the final states $\underline{L}(a_1)$ formed by the O $2p_z$ components of the apical oxygen O(apical) contributing to the molecular orbitals with the a_1 symmetry.

A schematic picture of the b_1, b_2, and a_1 molecular orbitals and the allowed polarized transitions from Cu $2p$ and O 1s are shown in Fig. 5.

B. Symmetry of calculated conduction bands

In order to define the symmetry of the calculated conduction bands, we discuss here the joint analysis of the calculated absorption cross sections in the ground state. The calculated polarized E⊥c Cu L_3-edge and Cu K-edge XANES spectra in Fig. 4(b) and the E∥c Cu L_3-edge and Cu K-edge XANES spectra in Fig. 4(c). The technical details on the Cu XANES spectra are discussed elsewhere.[38,40]

Following the dipole selection rule for polarized x-ray-absorption spectra $m_i+m_\gamma+m_f=0$ discussed above the calculated E⊥c Cu L_3-edge absorption $\alpha_\perp(\omega)$ is given by the sum of partial contributions $I_{l,m}$ to the absorption cross section due to final states with orbital angular momentum l,m:

$$\alpha_\perp(\omega)=I_{2,2}(\omega)+1/6I_{2,0}(\omega)+1/2I_{2,1}(\omega)\ ,$$

and the E∥c Cu L_3-edge absorption spectrum $\alpha_\parallel(\omega)$ is given by $\alpha_\parallel(\omega)=2/3I_{2,0}(\omega)+I_{2,1}(\omega)$. We can identify from Fig. 4 the presence of four bands ($i=0,1,2,3$) above the Fermi level that are schematically reported in Fig. 5.

The first band (with $i=0$) covers the energy from E_0 to 1 eV. At the Fermi level the Cu $2p\rightarrow 3d$ cross section in the Cu L_3-edge E⊥c polarized spectra has a sharp peak at E_0 due to the Cu ($l=2$, $m_l=\pm 2$) partial density of states. The calculated normalized absorption coefficient reaches the value $\alpha(\omega)/\alpha_0=290$ at the maximum to be compared with the range of values from 0 to 4 shown in Fig. 4.

This strong peak is due to the Cu $d_{x^2-y^2}$ band crossing the Fermi level, and its large intensity is due to the large overlap between the Cu $2p$ core level and the Cu $d_{x^2-y^2}$ orbital at the Cu site. The states of the $i=0$ band at the Fermi level also has oxygen $2p_x,2p_y$ character ($l=1$, $m_l=\pm1$) as is shown by the $\mathbf{E}\perp c$ O K-edge absorption cross section. The calculated $\mathbf{E}\|c$ Cu L_3-edge normalized absorption coefficient reaches the value $\alpha(\omega)/\alpha_0=15$ due to the tail of the Cu $d_{3z^2-r^2}$ partial density of states which extends beyond E_0 mostly because of the distortions in the CuO_4-square plane,[49] we find therefore at the Fermi level a 5% component with orbital angular momentum $m_l=0$, of the total Cu $3d$ holes in the mostly Cu $d_{x^2-y^2}$ band, $i=0$, crossing the Fermi level in the present one-electron electronic structure calculation using the real distorted Cu site structure.

The second band (with $i=1$) extends from ~1 to ~4 eV above E_0, this band can be identified with the band that is usually assigned to BiO layers in band-structure calculations.[29–33] The $\mathbf{E}\|c$ Cu L_3-edge spectrum exhibits the peak $C1$ due to the calculated partial density of states in the continuum ε with d-like symmetry and orbital angular momentum $m_l=0$. There is a large difference of the overlap between the Cu $2p$ atomic level with the Cu $3d$ states of the $i=0$ band and the Cu εd states in the continuum for bands $i=1,2,3$ as is demonstrated by the value of the Cu $2p\rightarrow d$ normalized absorption coefficient $\alpha(\omega)/\alpha_0$ going from 290 for the former states to 1–4 for the latter. This band has a relevant O $2p_{x,y}$ component as is shown by the peak $F1$ in the oxygen $\mathbf{E}\perp c$ K-edge spectrum. Therefore, these oxygen $2p$ states reached by oxygen K-edge spectra should have $\underline{L}(a_1)$ symmetry. Also the Cu $2p_z$ partial density of states contributes to this band as is demonstrated by peak $A1$ in the $\mathbf{E}\|c$ Cu K-edge spectrum.

The third band (with $i=2$) extends from 4 to 11 eV above E_0. It gives origin to the peaks $F2$ and $F3$ in the oxygen $\mathbf{E}\perp c$ K-edge spectrum, to the weak peaks $D1$ in the $\mathbf{E}\perp c$ Cu L_3-edge spectrum, to the structure $C2$ in the $\mathbf{E}\perp c$ Cu L_3-edge spectrum, and to the structure $A2$ in the $\mathbf{E}\|c$ Cu K-edge spectrum. The peak $C2$ in the $\mathbf{E}\|c$ Cu L_3 edge is given mainly by the $m_l=\pm1$ Cu d density of states in the continuum ε.[38] The peaks $F2$ and $F3$ show a relevant contribution of the O $2p_{x,y}$ orbitals. The peak $A2$ in the Cu K-edge spectrum shows the Cu $2p_z$ contribution to this band. We note that the present calculation predicts that the final states in the $i=2$ band can also be reached in the oxygen $\mathbf{E}\|c$ K-edge spectrum because of the predicted mixing of the O $2p_z$ orbitals of planar oxygens with the Cu d states with e symmetry.

The fourth band (with $i=3$) extends from 11 to 15 eV above E_0. This band gives only a well-defined peak in the $\mathbf{E}\perp c$ polarized Cu K-edge absorption spectrum, the main maximum $B1$, and a weak maximum is seen also in the Cu L_3-edge $\mathbf{E}\perp c$ polarized spectrum. The present calculation shows that this band has mainly Cu $\varepsilon p_{x,y}$ character. A schematic picture of the electronic structure of the conduction bands (with $i=0,1,2,3$) as derived by the present calculations is shown in Fig. 6.

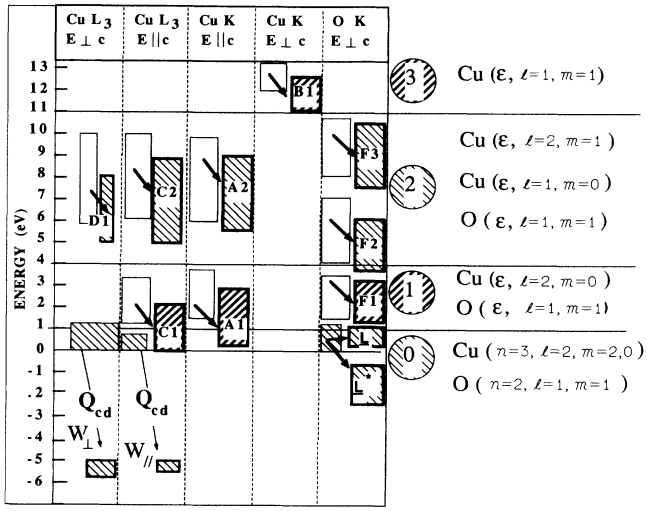

FIG. 6. Schematic picture of the final states reached by x-ray absorption from the oxygen and copper core levels. The open boxes indicate the positions of the final state as calculated in the unrelaxed potential. The horizontal lines divide the bands with $i=0$, 1, 2, and 3 above the Fermi level. On the right-hand side of the figure the main orbital contributions to the partial density of states for each band are given. The dashed boxes indicate the final states reached in the experimental x-ray-absorption spectra in Figs. 1–3.

C. The excitonic core-hole final-state effect on the XANES

In order to compare the experimental spectra with the one-electron calculations, we have included the perturbation of the final states induced by the core hole. The core-hole relaxation effect can be reduced to a one-electron problem by assuming that the potential seen by the photoelectron is the static potential where all passive electrons are fully relaxed in the presence of the core hole. According to the final-state rule, XANES spectra have to be calculated using the fully relaxed potential, closely approximated by that of the atom with its atomic number Z increased by 1 ($Z+1$ approximation).[42]

The oxygen K-edge polarized x-ray-absorption spectrum in the fully relaxed potential in the presence of the O $1s$ core hole is shown in Fig. 7(a). The oxygen K-edge spectrum is compared with the Cu L_3- and K-edge spectra calculated in the presence of a Cu $2p$ and $1s$ core hole, respectively, see Figs. 7(b) and 7(c).

The oxygen $1s$ core hole has a weak effect on the O $2p$ states of the $i=0$ and $i=1$ bands, moving the final states toward lower energies by only 0.5 eV, and a little larger effect on the peaks $F1$ and $F2$ inducing a red shift of about 1 eV.

The effect of the Cu $2p$ core hole, shown in Figs. 7(b) and 7(c) is much larger for the Cu $3d$ states in the $i=0$ band, moving the final states toward lower energies by 5.5 eV in agreement with the large overlap between the Cu $2p$ core and the Cu $3d$ valence states already discussed.

The effect of the Cu $2p$ core hole on the delocalized Cu εd final states is much smaller, ~1 eV, and it is similar to

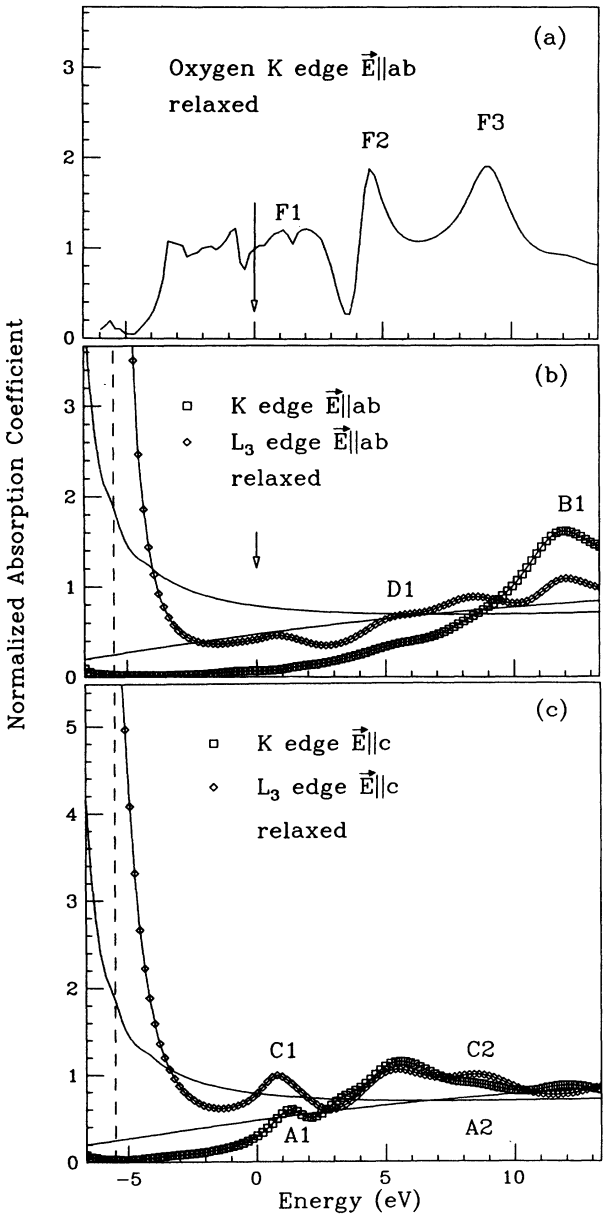

FIG. 7. (a) Calculated polarized E⊥c (E||ab plane) O K-edge XANES spectra of $Bi_2Sr_2CaCu_2O_8$ of the planar oxygen in the CuO_2 plane in the fully relaxed potential in the presence of the oxygen 1s hole. (b) Calculated polarized E⊥c (E||ab plane) Cu K-edge and Cu L_3 -edge XANES spectra in the fully relaxed potential in the presence of the copper 1s or 2p hole calculated by the $Z+1$ approximation. The atomic absorption spectra $\alpha_0(\omega)$ for the Cu $1s \rightarrow \varepsilon p$ and for the Cu $2p \rightarrow \varepsilon d$ transitions are plotted (solid lines). The zero of the energy scale is the Fermi level. (c) Calculated polarized E||c Cu K-edge and Cu L_3-edge XANES spectra of $Bi_2Sr_2CaCu_2O_8$ in the fully relaxed potential in the presence of the copper 1s or 2p hole obtained by using the $Z+1$ approximation. The atomic absorption spectra $\alpha_0(\omega)$ for the Cu $1s \rightarrow \varepsilon p$ and for the Cu $2p \rightarrow \varepsilon d$ transitions are plotted (solid lines). The zero of the energy scale is the calculated continuum threshold E_0 in the unrelaxed potential for one-electron calculated spectra as in Fig. 4.

the effect of the Cu 1s core hole on the Cu εp final states in the Cu K-edge spectrum. In conclusion, the Cu 2p core level induces an excitonic red shift on the Cu 3d final states of 5.5 eV that separates the Cu 3d final states from all other final states which are affected by the core hole for a nearly rigid shift of only 0.8–1.5 eV.

D. Comparison with experimental XANES features in the high-energy continuum

Figure 8 shows a comparison of the calculated XANES spectra with the five polarized spectra plotted in Figs. 1–3. The energy broadening due to the core hole and photoelectron lifetime[38] are included in the calculated fully relaxed absorption spectra of Fig. 7. Only the calculated absorption cross section to unoccupied states is plotted to be compared with experimental data. The zero of the energy scale is kept fixed at E_0, the calculated Fermi level in the one-electron unrelaxed calculations of Fig. 4. The experimental spectra are plotted in Fig. 8 by aligning the experimental XANES features in the high-energy range with the calculated XANES features in the range from 1 to 13 eV above E_0.

We can see that there is good agreement between the experimental and the calculated spectra for all final states beyond about 1 eV above E_0.

The comparison of the calculated O(planar) K-edge E⊥c polarized spectrum with the polarized experimental spectrum of Ref. 39 is satisfactory considering that the experimental features $F1$, $F2$, and $F3$ are correctly predicted. It is necessary to be reminded that the experimental spectrum is determined by eight oxygen atoms for one formula unit: the four equivalent planar oxygen sites O(planar) in the CuO_2 layers (for which the XANES calculation has been carried out), the two oxygen atoms in the SrO layers, and the two oxygens in the BiO layers. The main peaks $F2$ and $F3$ are assigned to the oxygen atoms in the plane because they are common to all cuprate perovskites with CuO_2 layers as shown by the oxygen K-edge spectra of both Nd_2CuO_4 and La_2CuO_4 (Ref. 50) and in $La_{1.85}Sr_{0.15}NiO_4$ (Ref. 51) exhibiting the peaks $F2$ in the range 533–535 eV and $F3$ in the range 537–540 eV. The peaks $F2$ and $F3$ in the experimental spectra are therefore assigned to final states in the $i=2$ band in Fig. 6. This band can be reached by polarized E||c Cu L_3-edge and K-edge spectra giving the broad spectral features $C2$ and $A2$, respectively, in Fig. 8(c). The $i=2$ band also gives a weak feature $D1$ in the E⊥c Cu L_3-edge spectrum.

The $i=3$ band with Cu $\varepsilon p_{x,y}$ character gives the main peak $B1$ in the E⊥c Cu K-edge spectrum, Fig. 8(b), and a broad maximum in the E⊥c Cu L_3-edge spectrum, Fig. 8(b), but it gives no contribution in the oxygen E⊥c K-edge spectrum in Fig. 8(a) and in the E||c spectra of copper levels in Fig. 8(c).

The $i=1$ band in Fig. 6 in the continuum ε, but only about 1.5–2 eV above E_0 with d-like character and $m_l=0$ orbital angular momentum is moved by the core-hole Coulomb final-state excitonic effect close to E_0. It gives origin to the following: (i) The peak $F1$ in the oxygen K-edge spectrum at about 2 eV above E_0 in Fig. 8(a)

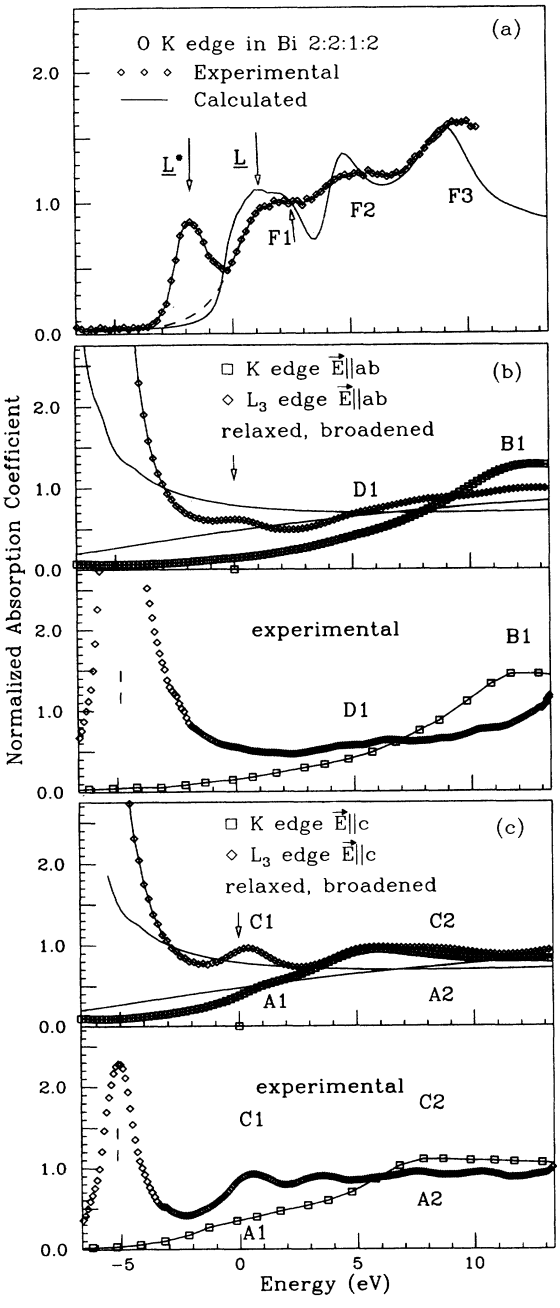

FIG. 8. (a) Calculated polarized E⊥c ($E\|ab$ plane) K-edge absorption spectra of the planar oxygen in the CuO_2 plane in $Bi_2Sr_2CaCu_2O_8$ for the fully relaxed potential in the presence of the oxygen 1s hole including the energy-dependent broadening (solid line) compared with the experimental oxygen 1s absorption spectra. (b) Calculated polarized E⊥c (E$\|ab$ plane) Cu K-edge and Cu L_3-edge XANES spectra in the fully relaxed potential including the energy-dependent broadening compared with the experimental spectra in the lower panel. (c) Calculated polarized E$\|c$ Cu K-edge and Cu L_3-edge XANES spectra of $Bi_2Sr_2CaCu_2O_8$ in the fully relaxed potential including the energy-dependent broadening compared with the experimental spectra in the lower panel. The zero of the energy scale is the calculated continuum threshold E_0 that corresponds to the calculated one-electron Fermi level in the unrelaxed potential in Fig. 4.

and at 532.5-eV photon energy in the experimental spectrum in Fig. 1. The peak $F1$ is unresolved from the peak ($\underline{L}$) due to oxygen 2p states at 531 eV in the experimental spectrum. The final state is unresolved from the spectral distribution of the oxygen $p_{x,y}$ density of states of the oxygen 2p band crossing the Fermi also in the one-electron calculation for the unrelaxed potential, see Fig. 4(a), where it appears as the structure $F1$ at about 2.5 eV above E_0. The calculated core-hole excitonic shift is only ~ 0.5 eV. (ii) The $i=0$ band gives origin also to the peaks $C1$ and $A1$ in the E$\|c$ Cu L_3 -edge and Cu K-edge spectra in Fig. 8(b) in both calculated and experimental spectra. The peak $A1$ appears at about E_0 and $C1$ at about 0.8 eV above E_0. The core-hole excitonic effect has moved these final states by about 1–1.5 eV from the position in the ground state. Therefore, the presence of the E$\|c$ components in both Cu edges shows that this $i=0$ band at about 1–2 eV above E_0 has components εp_z and εd_{z^2} at the Cu sites as predicted by the one-electron calculations reported here and summarized in Fig. 6.

E. The final states in the band around the Fermi level

The discussion of the final states in x-ray-absorption spectra rising from the electronic states in an energy range of about 1 eV around the Fermi level requires a separate discussion. In fact, we have seen that the calculation of the electronic states in the high-energy continuum within the one-electron approximation and the predictions of the final-state XANES features including the core-hole Coulomb final-state effect are in good agreement with the experimental results. Moreover, the excitonic shift for these final states in the continuum ε gives only a nearly rigid shift, therefore it is not difficult to extract direct information on the ground state from the experimental spectra.

The situation is twofold different for the final states in the range of 1 eV around the Fermi level, with $i=0$ in Fig. 6. In fact, the Cu 3d orbitals are localized at the atomic Cu site while the εd states in the high-energy bands (with $i=1,2,3$) are delocalized over a large cluster. This gives rise to, *first,* a large electronic correlation within the Cu 3d states $U_{dd} \sim 6\pm 2$ eV in the ground states, *second,* to a large Cu 2p, Cu 3d excitonic final state $U_{cd} \sim 5.5$ eV effect in the x-ray-absorption spectra.

The final states in the x-ray-absorption spectra have been discussed in the local-density band picture, with both disagreement[52] and agreement[53] with experiments reported, and within the Andersen impurity model[54] mainly for $YBa_2Cu_3O_{\sim 7}$.

The present calculation of the E⊥c O(planar) K-edge spectra, Fig. 8(b), shows a small excitonic final-state red shift for the calculated final states. This excitonic effect moves the calculated threshold by only 0.5 eV below E_0. The small value for the O 1s core hole and the O 2p valence is in agreement with other authors.[53,55] The experimental spectrum exhibits a minimum at E_0 with a peak at about -1.5–2 eV (the peak $\underline{L}^*$ at ~ 528 eV in the photon energy scale of Fig. 1) and a second peak $\underline{L}$ just above E_0 (the peak $\underline{L}$ at ~ 531 eV in the photon energy scale of Fig. 1).

The peak $\underline{L}$ is present both in the insulating ($Bi_2Sr_2YCu_2O_{8+\delta}$) and in the metallic phase,[12–14,17] and it decreases very slowly by increasing doping.[17,56] The peak $\underline{L}^*$ appears only in the hole-doped metallic phase.[17] By a comparison between the experimental and the calculated spectra in Fig. 8(a), we can ascribe the minimum at E_0 in the experimental spectra to the formation of a correlation gap of about 2 eV around E_0.

A correlation gap between the $3d_i^9+3d_j^9 \rightarrow 3d_i^{10}+3d_j^9\underline{L}_j$ opens up in the $3d$ band, due to the large Cu $3d$-$3d$ intra-atomic hole-hole Coulomb repulsion U_{dd} and for the Cu $3d$–O $2p$ interatomic Coulomb repulsion $V_{dp} \sim 1$ eV.[57] The correlation gap in the ionic limit is given by the $\Delta + V_{pd}$ where Δ is the energy separation between the $3d^9$ and the $3d^{10}\underline{L}$ configuration. The final state for the peak $\underline{L}$ in the oxygen K-edge absorption spectrum in the insulating case is the upper Hubbard band. In fact, the absorption process takes place at an atomic oxygen site where the electronic configuration will be described by mixing of $3d^9$ and the $3d^{10}\underline{L}$ configuration giving a single final state O $1s^1$–Cu $3d^{10}$ where an oxygen $2p$ hole (the ligand hole) is annihilated by creating the O $1s$ core hole. The intensity of the peak will be proportional to the probability of the $3d^{10}\underline{L}$ configuration (i.e., the number of ligand holes $\underline{L}$) in the initial state. This interpretation of the oxygen K edge of transition-metal oxide Mott insulators is similar to the one originally developed for the interpretation of the NiO spectrum[58,59] and later extended to doped NiO semiconductors.[60] The present results in Fig. 4(a) show that the position of the $3d^{10}$ final state occurs just above the Fermi level predicted by a one-electron calculation. The same result was already obtained for NiO from the analysis of the oxygen K-edge spectrum.[58]

In the doped metallic phase, an additional peak $\underline{L}^*$, not predicted by one-electron calculations, appears well below the predicted Fermi level at about 528 eV. This peak is broad extending over a range from about -2 eV to 0. The energy separation from the peak at 530–531 eV is of the same order of magnitude as the correlation gap in the insulating phase of 1.7 eV determined by optical spectroscopy.[35] This peak is assigned to the final states O $1s^1$–Cu $3d^9$ originating from the formation of the $3d^9\underline{L}^*$ states induced by doping. It is due to annihilation of one hole $\underline{L}^*$ and the creation of one O $1s$ core hole, therefore, its intensity probes the number of itinerant $\underline{L}^*$ induced by doping in agreement with analysis of the $La_{2-x}Sr_xCuO_4$ oxygen K-edge spectra.[55]

Information on the symmetry of the states $3d^9\underline{L}^*$ can be obtained by polarized x-ray-absorption spectra. The peak $\underline{L}^*$ at 528 eV in the metallic $Bi_2Sr_2CaCu_2O_{8+\delta}$ is observed only in the E$\perp c$ polarized oxygen K-edge spectrum.[12–14] Therefore, the oxygen orbitals $2p_z$ both of planar oxygens atoms O(planar), contributing to the $\underline{L}(e)$ orbitals, and of the apical oxygen atoms O(apical), contributing to the $\underline{L}(a_1)$ orbitals, do not contribute to the itinerant ligand hole $\underline{L}^*$ states.

While the presence of ligand hole states with symmetry e is completely ruled out by our work, the presence of ligand holes with a_1 symmetry is not ruled out because the planar O(planar) $2p_{x,y}$ orbitals can also be at the origin of the $\underline{L}(a_1)$ holes. Therefore, the polarized E$\perp c$ transition O $2p \rightarrow \underline{L}^*$ given the information that the symmetry of itinerant state can be of b_1, b_2, and a_1 symmetry but not of e symmetry (see Fig. 6). In fact, the probability of O(apical) $2p_z$ orbitals contributing to the $\underline{L}(a_1)$ orbitals depends on the distance Cu-O(apical) that determines the T(apical), i.e., the transfer integral between the Cu $3d_{3z^2-r^2}$ orbital and the oxygen $2p_z$ of O(apical).

The probability of the O(apical) $2p_z$ holes was found to be relevant in the 80-K phase $YBa_2Cu_3O_{\sim 7}$ (Ref. 15) where the Cu-O(apical) distance is very short 2.30 Å (Refs. 61–63) at 300 K (2.28 Å at 13 K); on the contrary, it was found to be negligible in the 60-K phase $YBa_2Cu_3O_{\sim 6.5}$ where the Cu-O(apical) distance is longer 2.38 Å.[61,62]

We would like to remark that the presence of holes on the apical oxygen orbital can be associated with the variation of the ratio $r = d_{\text{Cu-O(apical)}}/d_{\text{Cu-O(planar)}}$. The ratio r is 1.18 in $YBa_2Cu_3O_{\sim 7}$ and $r = 1.16$ (Ref. 64) in the $3d^8$ compound $La_{2-x}Sr_xNiO_4$,[51] to be compared with $r = 1.23$ for $YBa_2Cu_3O_{\sim 6.5}$, $r \sim 1.28$ for $La_{2-x}Sr_xCuO_4$ where no holes in apex $2p_z$ orbitals have been found. In Bi 2:2:1:2 the Cu-O(apical) distance is not well defined in the literature but we can assume that the ratio r is larger than 1.18 if no holes are observed on the apex oxygen $2p_z$ orbitals. This result is in agreement with the diffraction data of Bi 2:2:1:2 giving $r \sim 1.3$.[65]

Following the rigid-band model (or three-band Hubbard model) (Refs. 9–11), a single final state O $1s^1$–Cu $3d^9_{x^2-y^2}$ gives rise to the 528-eV peak, for the models assuming a nonrigid electronic structure or multiband models[15–23] the final states O $1s^1$–Cu $3d^9_{x^2-y^2}$ and O $1s^1$–Cu $3d^9_{3z^2-r^2}$ will contribute to the 528-eV peak. This peak is very broad and does not show splitting; therefore, it is possible to put only a limit of about 0.5 eV for the energy splitting between these two possible final states.

The information on the symmetry of the Cu $3d$ holes can be obtained by the polarized Cu L_3 edge shown in Fig. 2. The excitonic final-state effect of the core hole is such that the $3d$ states are pushed down by $U_{cd} = 5.5$ eV in spite of the metallic screening.[54] The experimental data show this effect clearly because the ~ 5–6 eV energy splitting between the white line and the peak $C1$ is in agreement with the calculations in the fully relaxed potential, while it is in disagreement with the calculated splitting of about 1 eV in the unrelaxed potential.

The polarization dependence of the white line shown in Fig. 2 shows a relevant contribution of the Cu $3d$ orbitals oriented out of the CuO_2 plane, along the c axis. Following the dipole selection rules (see Fig. 6) and considering that the presence of unoccupied molecular orbitals with e symmetry has been ruled out between the three possible symmetries b_1, a_1, and b_2 left from the in-plane polarized O $1s \rightarrow \underline{L}^*$ transitions, the out-of-plane component of the Cu L_3 edge probes only the out-of-plane component of the Cu $3d^9_{3z^2-r^2}$ holes. Because the out-of-plane component of the white line in Cu L_3-edge spectra increases from 7% of the total integral of the nonpolarized in the

insulating $Bi_2Sr_2YCu_2O_8$ phase to 15~20 % in the metallic Bi 2:2:1:2 samples,[16,38] we assign the increase of about 10% of this component to Cu $3d^9_{3z^2-r^2}\underline{L}$ states formed with doping. The presence of the Cu $3d^9_{x^2-y^2}\underline{L}$ states is shown by the additional states forming with doping in the gap between the white line and the Fermi level. This gives origin to the asymmetric high-energy tail of the white line in the metallic phase that in the insulating phase shows a symmetric line shape.

In conclusion, the combined analysis of the Cu and oxygen K-edge spectra shows the presence of both Cu $3d^9_{x^2-y^2}\underline{L}^*$ and Cu $3d^9_{3z^2-r^2}\underline{L}$ probed by Cu L_3 absorption and $3d^9\underline{L}(b_1)$ and $3d^9\underline{L}(a_1)$ by oxygen K-edge spectra. However, only planar oxygen $2p_{x,y}$ orbitals contribute to the $\underline{L}(a_1)$ molecular orbitals, where the transfer integral $T(a_1)=(1/\sqrt{3})T(b_1)+T$ (apical) is mainly determined by the hybridization with the O $2p_{x,y}$ plane orbitals $(1/\sqrt{3})T(b_1)$ with a negligible contribution due to the hybridization T(apical) with the O(apical) $2p_z$ orbitals.

The energy splitting between the two polarized white lines can be associated in the language of the electronic cluster configurations with the energy separation between two possible final states Cu $2p^5\underline{L}(a_1)$ and Cu $2p^5\underline{L}(b_1)$ that will probe the energy separation $\Delta_{\underline{L}}$ between $\underline{L}(a_1)$ and $\underline{L}(b_1)$ states considered to be a key term by some theoretical models for high-T_c superconductors.[66,67]

III. CONCLUSIONS

The one-electron calculation of the partial and local density of states of the high-energy conduction bands in the range beyond 1 eV above the Fermi level are in good agreement with the polarized x-ray-absorption spectra at both the copper and oxygen edges. The scheme of the energy distribution of the high-energy bands, shown in Fig. 5, obtained by the present study is in agreement with the vacuum ultraviolet reflectivity data[35] and the electron-energy-loss data.[36]

The presence of a band in the continuum above the Fermi level with maxima in the partial and local density of states only ~1 eV above the calculated Fermi level E_0 is found. This band, usually assigned to the BiO layer in band-structure calculations,[29–33] is shown here to have a relevant component in the CuO_2 plane with Cu εd $m_l=0$ (peak $C1$ in Cu L_3 edge), εp $m_l=0$ (peak $A1$ in Cu K edge), and O $2p_{x,y}$ (peak $F1$ in O K edge). Considering the fact the BiO band has been found to cross the Fermi level at the M point (where a Van Hove singularity is expected) by angle-revolved photoemission,[28] we think that this band can play in the Bi 2:2:1:2 system a similar role to the chain band in $YBa_2Cu_3O_{\sim 7}$.

Finally, the symmetry of the $3d$ and O $2p$ hole states at the Fermi level contributing to the $3d^9\underline{L}^*$ states induced by doping has been found to have Cu $3d^9_{x^2-y^2}$, and Cu $3d^9_{3z^2-r^2}$ symmetry probed by Cu L_3 absorption and in O $2p$ in-plane components of $\underline{L}(b_1)$ and $\underline{L}(a_1)$ symmetries. These results show a breakdown of the rigid-band electronic structure with doping assumed in the three-band Hubbard model and support the nonrigid-band models. The relevant contributions of Cu $3d^9_{3z^2-r^2}$ and $\underline{L}(a_1)$ partial density of unoccupied states to the band crossing the Fermi level show the presence of a band of $3d_{3z^2-r^2}$ character very close or crossing the Fermi level in agreement with several models of the electronic structure of high-T_c superconductors.[48,66,18–23]

ACKNOWLEDGMENTS

We are grateful to A. Krol and Y. H. Kao for sending us the oxygen K-edge absorption spectra before publication. We would like to thank the Consorzio Interuniversitario Nazionale per la Fisica della Materia (INFM) and the Progetto Finalizzato per la Superconduttività del Consiglio Nazionale delle Ricerche for supporting this research. On of us (C.Li) would like to thank the International Center for Theoretical Physics and the Consorzio Interuniversitario Nazionale per la Fisica della Materia for support during his stay in Italy.

*Permanent address: Institute of Physics, Academia Sinica, Beijing, China.

[1]A. Fujimori, E. Takayama-Muromachi, Y. Uchida, and B. Okai, Phys. Rev. B **35**, 8814 (1987).

[2]A. Bianconi, A. Congiu Castellano, M. De Santis, P. Delogu, A. Gargano, and R. Giorgi, Solid State Commun. **63**, 1135 (1987).

[3]Z. X. Shen, J. W. Allen, J.-J. Yeh, J. S.-S. Kang, W. Elis, W. E. Spicer, I. Lindau, M. B. Maple, Y. D. Dalichaouch, M. S. Torikachvili, J. Z. Sun, and T. H. Geballe, Phys. Rev. B **36**, 8414 (1987).

[4]W. E. Pickett, Rev. Mod. Phys. **61**, 433 (1989).

[5]*High-T_c Superconductors: Electronic Structure, Proceedings of the International Symposium on the Electronic Structure of High-T_c Superconductors, Roma, 1988,* edited by A. Bianconi and A. Marcelli (Pergamon, Oxford, 1989).

[6]*Earlier and Recent Aspects of Superconductivity,* edited by K. A. Müller and J. G. Bednorz, Springer Series in Solid State Sciences (Springer-Verlag, Berlin, 1990).

[7]A. Bianconi, A. Congiu Castellano, M. De Santis, P. Rudolf, P. Lagarde, A. M. Flank, and A. Marcelli, Solid State Commun. **63**, 1009 (1987).

[8]A. Bianconi, J. Budnick, A. M. Flank, A. Fontaine, P. Lagarde, A. Marcelli, H. Tolentino, B. Chamberland, C. Michel, B. Raveau, and G. Demazeau, Phys. Lett. **127**, 285 (1988).

[9]V. J. Emery, Phys. Rev. Lett. **58**, 3759 (1987); C. M. Varma, S. Schmitt-Rink, and E. Abrahams, Solid State Commun. **62**, 681 (1987).

[10]A. K. McMahan, R. M. Martin, and S. Satpathy, Phys. Rev. B **38**, 6650 (1988); J. F. Annet. R. M. Martin, A. K. McMahan, and S. Satpathy, *ibid.* **40**, 2620 (1989); M. S. Hybertsen, M. Schluter, and N. E. Christensen, *ibid.* **39**, 11 445 (1989).

[11]F. C. Zhang and T. M. Rice, Phys. Rev. B **37**, 3759 (1988); H. Eskes and G. A. Sawatzky, Phys. Rev. Lett. **61**, 1415 (1988).

[12]F. J. Himpsel, G. V. Chandrasekhar, A. B. McLean, and M.

W. Shafer, Phys. Rev. B **39**, 2926 (1989).
[13]N. Nüker, H. Romberg, X. X. Xi, J. Fink, B. Gegenheimer, and Z. X. Zhao, Phys. Rev. B **39**, 6619 (1989).
[14]P. Kuiper, M. Grioni, G. A. Sawatzky, D. B. Mitzi, A. Kapitulnik, A. Santaniello, P. de Padova, and P. Thiry, Physica C **157**, 260 (1989).
[15]A. Bianconi, M. De Santis, A. M. Flank, A. Fontaine, P. Lagarde, A. Marcelli, H. Katayama-Yoshida, and A. Kotani, Physica C **153-155**, 1760 (1988); Phys. Rev. B **38**, 7196 (1988).
[16]A. Bianconi, P. Castrucci, A. M. Flank, P. Lagarde, S. Della Longa, A. Marcelli, H. Katayama-Yoshida, and Z. X. Zhao, Mod. Phys. Lett. B **2**, 1313 (1988); A. Bianconi, P. Castrucci, A Fabrizi, M. Pompa, A. M. Flank, P. Lagarde, H. Katayama-Yoshida, and G. Calestani, Physica C **162-164**, 209 (1989); *Earlier and Recent Aspects of Superconductivity,* edited by K. A. Müller and J. G. Bednorz, Springer Series in Solid State Sciences (Springer-Verlag, Berlin, 1990), p. 407; A. Bianconi, in *Proceedings of the International Conference on Superconductivity -ICSC, Bangalore, 1990,* edited by S. K. Joshi, C. N. R. Rao, and S. V. Subranyam (World-Scientific, Singapore, 1990), p. 448.
[17]H. Matsuyama, T. Takahashi, H. Katayama-Yoshida, T. Kashiwakura, Y. Okabe, S. Sato, N. Kosugi, A. Yagishita, K. Tanaka, H. Fujmoto, and H. Inokuchi, Physica C **160**, 567 (1989).
[18]C. Castellani, C. Di Castro, and M. Grilli, Physica C **153-155**, 1659 (1988); Int. J. Mod. Phys. **1**, 659 (1988).
[19]H. Kamimura, Int. J. Mod. Phys. **1**, 699 (1988).
[20]S. Kurihara, Physica C **153-155**, 1247 (1988); T. Nishnio, M. Kikuchi, and J. Kanamori, Solid State Commun. **68**, 455 (1988); V. V. Flambaum and O. P. Sushkov, Physica C **159**, 595 (1989).
[21]R. Englman, B. Halperin, and M. Weger, Solid State Commun. **70**, 57 (1989); J. Ruvalds, Phys. Rev. B **35**, 8869 (1987).
[22]J. Askenazi and C. G. Kuper, Physica C **153-155**, 1315 (1988); J. Askenazi and C. G. Kuper, in *High-T_c Superconductors: Electronic Structure,* edited by K. A. Müller and J. G. Bednorz, Springer Series in Solid State Sciences (Springer-Verlag, Berlin, 1989), p. 43; W. Weber, Z. Phys. B **70**, 323 (1988).
[23]W. Weber, Adv. Solid State Phys. **28**, 141 (1988); A. L. Shelankov, X. Zotos, and W. Weber, Physica C **153-155**, 1307 (1988); Yu B. Gaididei and V. M. Loktev, Phys. Status Solidi B **147**, 307 (1988); M. Jarrell, H. R. Krishnamurthy, and D. L. Cox, Phys. Rev. B **38**, 4584 (1988); D. L. Cox, M. Jarrell, C. Jayaprakash, H. R. Krishna-murthy, and J. Diez, Phys. Rev. Lett. **62**, 2188 (1989).
[24]J. G. Bednorz and K. A. Müller, Z. Phys. B **64**, 189 (1986); Rev. Mod. Phys. **60**, 565 (1988).
[25]T. Takahaski, H. Matsuyama, H. Katayama-Yoshida, Y. Okabe, S. Hosoya, K. Seki, H. Fujimoto, M. Sato, and H. Inokuchi, Nature **334**, 691 (1988); Phys. Rev. B **39**, 6636 (1989).
[26]R. Manzke, T. Buslaps, R. Claessen, M. Skibowski, and J. Fink, Physica C **162-164**, 1381 (1989).
[27]C. G. Olson, R. Liu, A.-B. Yang, D. W. Lynch, A. J. Arko, R. S. List, B. W. Veal, Y. C. Chang, P. Z. Jiang, and A. P. Pauliskas, Science **245**, 731 (1989).
[28]B. O. Wells, Z.-X. Shen, D. S. Dessau, W. E. Spicer, C. G. Olson, D. B. Mitzi, A. Kapitulnik, R. S. List, and A. Arko, Phys. Rev. Lett. **65**, 3056 (1990).
[29]M. S. Hybertsen and L. F. Mattheis, Phys. Rev. Lett. **60**, 1661 (1988).
[30]H. Krakauer and W. E. Pickett, Phys. Rev. Lett. **60**, 1665 (1988).
[31]S. Masidda, J. Yu, and A. J. Freeman, Physica C **152**, 251 (1988); P. Marksteiner, S. Massida, J. Yu, A. J. Freeman, and J. Redinger, Phys. Rev. B **38**, 5098 (1988).
[32]F. Herman, R. V. Kasowski, and W. Y. Hsu, Phys. Rev. B **38**, 204 (1988).
[33]B. Szpunar and V. H. Smith, Jr., Phys. Rev. B **37**, 2338 (1988); B. Szpunar, V. H. Smith, Jr., and R. W. Smith, J. Mol. Struct. **202**, 347 (1989).
[34]P. Calvani, M. Capizzi, S. Lupi, P. Maselli, D. Peschiaroli, and H. Katayama-Yoshida, Solid State Commun. **74**, 1333 (1990).
[35]I. Terasaki, T. Nakahashi, S. Takebayashi, A. Maeda, and K. Uchinokura, Physica C **165**, 152 (1990).
[36]J. Fink, N. Nücher, H. Romberg, and N. Nakai, in *High-T_c Superconductors: Electronic Structure, Proceedings of the International Symposium on the Electronic Structure of High-T_c Superconductors, Roma, 1988* (Ref. 5), p. 293.
[37]R. Claessen, R. Manzke, H. Carstensen, B. Burandt, T. Buslaps, M. Skibowski, and J. Fink, Phys. Rev. B **80**, 181 (1990); J. Fink, N. Nücher, H. Romberg, M. Alexander, P. Adelmann, R. Claessen, G. Mante, T. Buslaps, S. Harm, R. Manzke, and M. Skibowski (unpublished).
[38]A. Bianconi, C. Li, M. Pompa, A. Congiu-Castellano, S. Della Longa, D. Udron, A. M. Flank, and P. Lagarde, Phys. Rev. B **44**, 10 126 (1991).
[39]A. Krol, C. S. Lin, Z. H. Ming, C. J. Sher, Y. H. Kao, C. T. Chen, F. Sette, Y. Ma, G. C. Smith, Y. Z. Zhu, and D. T. Shaw, Phys. Rev. B **42**, 2635 (1990).
[40]A. Bianconi, C. Li, F. Campanella, S. Della Longa, I. Pettiti, M. Pompa, S. Turtù, and D. Udron, Phys. Rev. B **44**, 4560 (1991).
[41]A. Bianconi, in *X-ray Absorption: Principles, Applications, Techniques of EXAFS, SEXAFS, and XANES,* edited by D. C. Koningsberger and R. Prinz (Wiley, New York, 1988), p. 573.
[42]P. J. Durham, in *X-ray Absorption: Principles, Applications, Techniques of EXAFS, SEXAFS, and XANES* (Ref. 41) p. 53.
[43]A. Bianconi, M. Dell'Ariccia, P. J. Durham, and J. B. Pendry, Phys. Rev. B **26**, 6502 (1982).
[44]P. J. Durham, J. B. Pendry, and C. H. Hodges, Comput. Phys. Commun. **25**, 193 (1982).
[45]D. D. Vvedensky, D. K. Saldin, and J. B. Pendry, Comput. Phys. Commun. **40**, 421 (1986).
[46]A. Bianconi, J. Garcia, and M. Benfatto, in *Synchrotron Radiation in Chemistry and Biology I,* edited by E. Mandelkow, Topics in Current Chemistry Vol. 145 (Springer-Verlag, Berlin, 1988), pp. 29-67.
[47]P. Bordet, J. J. Capponi, C. Chaillout, A. W. Hewat, E. A. Hewat, J. L. Houdeau, M. Marezio, J. L. Tholence, and D. Tranqui, Physica C **156**, 189 (1988).
[48]M. Grilli, C. Castellani, and C. Di Castro, Phys. Rev. B **42**, 6233 (1990).
[49]Y. Seino, A. Kotani, and A. Bianconi, J. Phys. Soc. Jpn. **59**, 815 (1990).
[50]A. Krol, C. S. Lin, Z. H. Ming, Y. H. Kao, C. L. Lin, S. L. Qui, J. Chen, J. M. Tranquada, M. Strongin, G. C. Smith, Y. K. Tao, R. L. Meng, P. H. Hor, C. W. Chu, G. Cao, and J. E. Crow, Phys. Rev. B **42**, 4763 (1990); (private communication).
[51]P. Kuiper, J. van Elp, G. A. Sawatzky, A. Fujmori, and D. M. de Leeuw (unpublished).
[52]N. Nüker, J. Fink, J. C. Fuggle, P. J. Durham, and W. M. Temmerman, Phys. Rev. B **37**, 5158 (1988).
[53]J. Zaanen, M. Aluani, and O. Jepsen, Phys. Rev. B **40**, 837 (1989).
[54]K. Okada and A. Kotani, J. Phys. Soc. Jpn. **58**, 2578 (1989); Y. Seino, K. Okada, and A. Kotani, *ibid.* **59**, 1384 (1990).

[55]C. T. Chen, F. Sette, Y. Ma, M. S. Hybertsen, E. B. Stechel, W. M. C. Foulkes, M. Schluter, S.-W. Cheong, L. W. Rupp, Jr., B. Batlogg, Y. L. Soo, Z. H. Ming, A. Krol, and Y. H. Kao, Phys. Rev. Lett. **66**, 104 (1991).

[56]A. Krol *et al.* (unpublished).

[57]M. De Santis, A. Bianconi, A. Clozza, P. Castrucci, A. Di Cicco, M. De Simone, A. M. Flank, P. Lagarde, J. Budnick, P. Delogu, A. Gargano, R. Giorgi, and T. D. Makris, in *High-T_c Superconductors: Electronic Structure, Proceedings of the International Symposium on the Electronic Structure of High-T_c Superconductors, Roma, 1988* (Ref. 5), p. 313.

[58]I. Davoli, A. Marcelli, A. Bianconi, M. Tomellini, and M. Fanfoni, Phys. Rev. B **33**, 2979 (1986).

[59]S. I. Nakai, T. Mitsuishi, H. Sugamara, H. Maezama, T. Matsukama, S. Mitani, K. Tamasaki, and T. Fujikama, Phys. Rev. B **36**, 9241 (1987).

[60]P. Kuiper, G. Kruizinga, J. Ghijpsen, G. A. Sawatzky, and H. Werweij, Phys. Rev. Lett. **62**, 221 (1989).

[61]J. J. Capponi, C. Chaillout, A. W. Hewat, P. Lejay, M. Marezio, N. Nguyen, B. Raveau, J. L. Soubeyroux, J. L. Tholence, and R. Tournier, Europhys. Lett. **3**, 1301 (1987).

[62]R. J. Cava, A. W. Hewat, E. A. Hewat, B. Batlogg, M. Marezio, K. Rabe, J. J. Krajewski, W. E. Peck, Jr., and L. W. Rupp, Jr., Physica C **165**, 419 (1990).

[63]G. H. Kwei, A. C. Larson, W. L. Hults, and J. L. Smith, Physica C **169**, 217 (1990).

[64]J. D. Jorgensen, B. Dabrowski, S. Pei, D. R. Richards, and D. G. Hinks, Phys. Rev. B **40**, 2187 (1989).

[65]A. I. Beskrovnyi, M. Dlouha, Z. Kirak, and S. Vratislav, Physica C **171**, 19 (1990); M. Onoda and M. Sato, Solid State Commun. **67**, 799 (1988).

[66]Y. Ohta, T. Tohyama, and S. Maekawa, Physica C **166**, 385 (1990).

[67]C. Di Castro, L. F. Feiner, and M. Grilli, Phys. Rev. Lett. **66**, 3209 (1991).

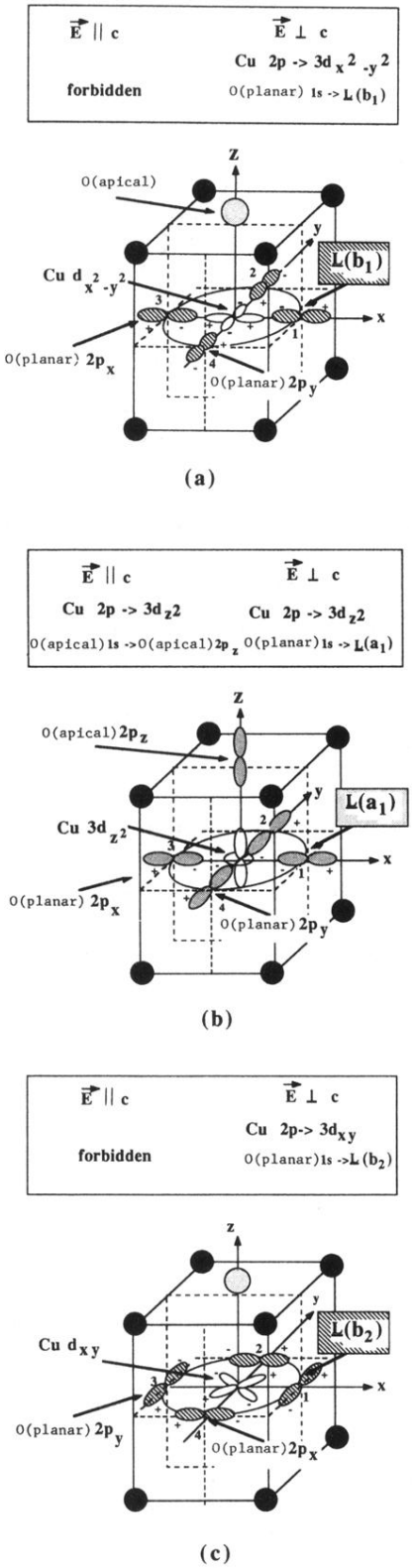

FIG. 5. Schematic picture of the final valence-band states of symmetry (a) b_1, (b) a_1, and (c) b_2 that can be reached with polarized Cu L_3-edge and O K-edge absorption.